Probing Resonant Photoionization Time Delay by Self-Referenced Molecular Attoclock

Jihong Tong,[1,*] Xiwang Liu,[2,*] Wenhui Dong,[3] Wenyu Jiang,[1] Ming Zhu,[2] Yidan Xu,[1] Zitan Zuo,[1] Peifen Lu,[1] Xiaochun Gong,[1,5,†] Xiaohong Song,[2] Weifeng Yang,[2,‡] and Jian Wu[1,4,5,6,§]

[1]*State Key Laboratory of Precision Spectroscopy, East China Normal University, Shanghai 200241, China*
[2]*School of Science and Center for Theoretical Physics, Hainan University, Haikou 570288, China*
[3]*Department of Physics, College of Science, Shantou University, Shantou, Guangdong 515063, China*
[4]*Chongqing Key Laboratory of Precision Optics, Chongqing Institute of East China Normal University, Chongqing 401121, China*
[5]*Collaborative Innovation Center of Extreme Optics, Shanxi University, Taiyuan, Shanxi 030006, China*
[6]*CAS Center for Excellence in Ultra-intense Laser Science, Shanghai 201800, China*

(Received 1 November 2021; revised 28 March 2022; accepted 23 September 2022; published 18 October 2022)

Attosecond time-resolved electron tunneling dynamics have been investigated by using attosecond angular streaking spectroscopy, where a clock reference to the laser field vector is required in atomic strong-field ionization and the situation becomes complicated in molecules. Here we reveal a resonant ionization process via a transient state by developing an electron-tunneling-site-resolved molecular attoclock in Ar-Kr$^+$. Two distinct deflection angles are observed in the photoelectron angular distribution in the molecular frame, corresponding to the direct and resonant ionization pathways. We find the electron is temporally trapped in the Coulomb potential wells of the Ar-Kr$^+$ before finally releasing into the continuum when the electron tunnels through the internal barrier. By utilizing the direct tunneling ionization as a self-referenced arm of the attoclock, the time delay of the electron trapped in the resonant state is revealed to be 3.50 ± 0.04 fs. Our results give an impetus to exploring the ultrafast electron dynamics in complex systems and also endow a semiclassical presentation of the electron trapping dynamics in a quantum resonant state.

DOI: 10.1103/PhysRevLett.129.173201

Tracing electron dynamics in real time is central to the understanding and exploring of the fundamental photophysical [1–4] and photochemical processes [5]. Attosecond metrology [6], such as the reconstruction of attosecond beating by interference of two-photon transitions [7], the photoelectron kinetic energy [8,9], and angular streaking spectroscopy [10], has been employed to clock the photoelectron emission time delay in strong-field ionization [11–15] and perturbation regime [9]. The observed attosecond time delay is raised by the interaction of the outgoing electronic wave packet with the ionic Coulomb potential [6,16] and also the transient trapping of the electron in a potential barrier constructed by an excited state [12,17] or a high angular momentum partial wave in continuum [18,19].

The resonant time delay is generally introduced when the electron is trapped temporarily in a resonant state for a period of time. As compared to the atomic resonant time delay [12,13,20] and the molecular shape resonance in continuum [18,19], the investigation of the molecular intermediate state assisted resonant time delay imposes more challenges. The congestion of multiple ionization channels makes the photoionization dynamics complex [21], the neighboring ionic cores could alter the electronic motion resulting in intramolecular charge rearrangement [4,22], enhanced ionization [23–25], and averaging effects due to molecular orientation [26,27] increase the complexity of photoionization time delay measurements in molecules.

In this Letter, we introduce a self-referenced asymmetric molecular attoclock to investigate the resonant photoionization dynamics in a heteronuclear van der Waals complex of Ar-Kr [28–36]. The unique properties of the rare gas dimer are the atomic structure of each subunit, the extraordinarily large internuclear distance as compared to diatomic molecules, and the absence of fully delocalized molecular orbitals. The intrinsic electron localization of the highest occupied molecular orbital of Ar-Kr provides a preference for the electron removal from the Kr atom side in the first ionization step by the pump pulse. The site-resolved electron hole in the pump pulse prepared Ar-Kr$^+$ at large internuclear separation guarantees that the second electron is mainly removed from the Ar atom side, which provides a prototype system to investigate the electron tunneling dynamics of a neutral atom neighboring a Coulomb potential. As illustrated in Fig. 1, in addition to the direct tunneling ionization through the outer barrier [see Fig. 1(a)], the electron has a large probability to tunnel through the internal barrier and is trapped within the potential well forming a trapping state, as shown in Fig. 1(c). We reveal that ionization via the trapped state [see Fig. 1(d)] is one of the origins of the enhanced ionization in molecules [23–25,37]. Under the protocol

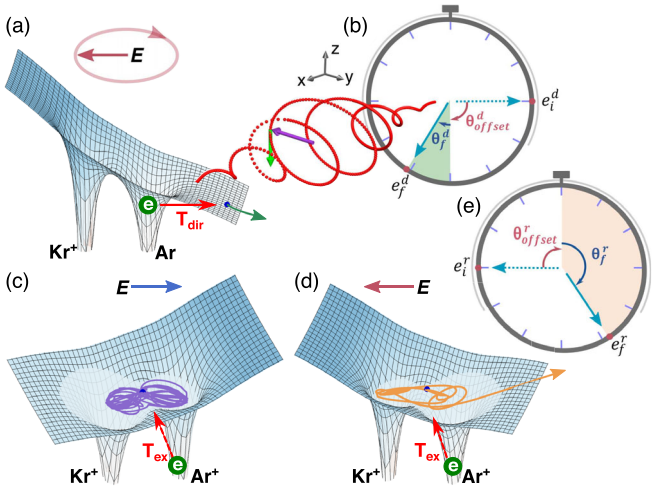

FIG. 1. (a) Schematic diagram of the direct tunneling ionization pathway, where the electron is released from the argon atom side. The red arrow with T_{dir} indicates the tunneling process, and the green curve is the typical electron trajectory. (b) The stopwatch of the direct electron tunneling process, where e_i^d and e_f^d indicate the initial and final momentum directions, θ_f^d indicates the electron tunneling deflection angle, and $\theta_{\mathrm{offset}}^d$ is the streaking angle from the laser field. Schematic diagram of (c) Coulomb trapping and (d) resonant ionization process, where the red arrow labeled with T_{ex} indicates the nonadiabatic excitation process, the purple and yellow curves are the electron trajectories, and the blue dot is the electron tunneling exit. (e) The stopwatch of the resonant ionization pathway. Arrows are labeled the same as (b) but for the resonant ionization pathway.

of the attoclock [10], the final momentum of the direct tunneling electron is deflected into the vector of e_f^d in Fig. 1(b), and the total angular shift can be divided into a vector potential induced deflection $\theta_{\mathrm{offset}}^d = 90°$ and an electron ionization term θ_f^d (the green area), which includes the tunneling and the subsequent propagation in the laser-Coulomb coupled field [38–40]. The trapping time of the electron in the intermediate state is revealed to be 3.50 ± 0.04 fs by taking the direct tunneling electron as a "timing reference" of the molecular attoclock.

Experimentally, the Ar-Kr dimer was generated via a supersonic expansion of a mixture of He (10%), Ar (70%), and Kr (20%) through a 30-μm nozzle. The ultrashort femtosecond laser pulse (25 fs, 800 nm, 10 kHz) was split into two pulses to build a noncollinear Mach-Zehnder interferometer. The wavelength of the pump and probe laser pulses are central at 800 nm, and the laser beam was tightly focused onto the supersonic gas jet by using a concave sliver mirror ($f = 7.5$ cm) inside the cold target recoil ion momentum spectroscopy [41,42]. The linearly polarized pump pulse along the y axis is adopted to prepare the Ar-Kr$^+$. The created vibrational nuclear wave packet of Ar-Kr$^+$ starts to move after the single ionization of Ar-Kr, and a 300 fs time delayed intense elliptically polarized probe pulse is used to remove the second electron. The measured ionic kinetic energy release distribution (3.72 eV) [43] shows that the internuclear separation of Ar-Kr$^+$ at the moment of ionization with the time delayed elliptical probe pulse is about 3.9 Å within the Franck-Condon transition region, where the highest occupied molecular orbital of Ar-Kr$^+$ is mainly localized at the argon atom side (see Fig. S3 in the Supplemental Material [43]). This guarantees that the second electron is mainly removed from the Ar atom side. As shown in Fig. 2(a), the linearly polarized pump pulse contributes a fusiform distribution of photoelectron momentum along the py_e axis with $|pz_e| \leqslant 0.2$ a.u., indicated by the parallel areas of white dashed lines. The probe laser pulse rotated clockwise from $+z$ to $+y$ in the y–z plane and propagated along the $-x$ axis after the focusing mirror. Owing to the angular streaking effect [10] of the probe pulse, the photoelectron momentum can be deflected with $|pz_e| > 0.2$ a.u., indicated by the white dashed sectors [see Fig. 2(b)]. The different properties of pump and probe fields including the polarization and intensity, together with the coincident detection of electrons and ions, allow us to identify the pump-probe signal from that of double ionization by one pulse of either the pump or the probe field (see details in Supplemental Material [43] and Refs. [59–62]). The peak intensities of the pump and probe laser pulse in the interaction region and the ellipticity of the probe pulse were estimated to be $I_{\mathrm{pump}} \sim 0.75 \times 10^{14}\,\mathrm{W/cm^2}$, and $I_{\mathrm{probe}} \sim 0.85 \times 10^{14}\,\mathrm{W/cm^2}$, and $\epsilon_{\mathrm{probe}} = 0.8$, respectively.

Figures 2(c) and 2(d) show the measured and simulated electron momentum distributions released by the elliptically polarized probe pulse with the Ar-Kr$^+$ nuclear orientation along with a positive y axis. The simulations employ an improved Coulomb-corrected strong-field approximation (CCSFA) with internuclear separation $R_{\mathrm{Ar-Kr}} = 3.9$ Å [13,63–65], which compare well with the experimentally measured results. Both of the measured and simulated photoelectron angular distributions (PADs) show two deflection peaks at $-54° \pm 5°$ and $-122° \pm 5°$, as the integrated PADs presented in Fig. 2(e).

To get an insight into the electron tunneling dynamics of the Ar atom neighboring the Coulomb potential of the Kr$^+$, we performed a semiclassical statistical trajectory analysis. In this model, the initial conditions of the electron trajectories at the tunneling exit are calculated by the saddle-point method [38,43,65,66], and then the electron is propagated in the laser-Coulomb coupled fields (see Supplemental Material [43]). The blue line in Fig. 3(a) shows the probability distribution of the electron as a function of initial total energy, i.e., the sum of kinetic and potential energy distribution of the involved trajectories at the tunneling exit ($E_{\mathrm{ini}}^{\mathrm{tot}}$). The typical electron trajectories with $E_{\mathrm{ini}}^{\mathrm{tot}} \sim -0.15$ a.u. are dominated by the direct tunneling process via the outer barrier, as shown in Fig. 1(a). The electron trajectories with $E_{\mathrm{ini}}^{\mathrm{tot}} \sim -0.40$ a.u. correspond to a

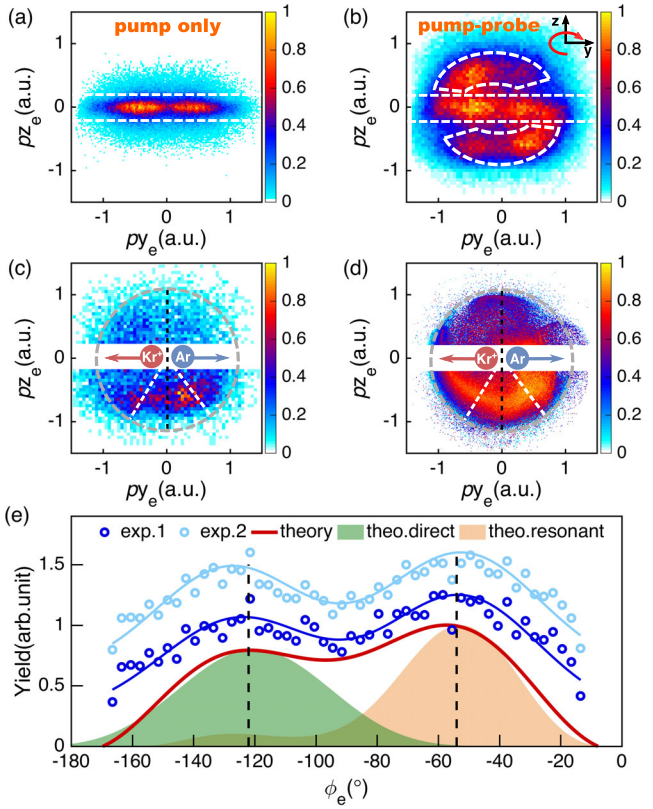

FIG. 2. (a) Experimentally measured electron momentum distribution recorded by the pump pulse alone. The parallel areas of white dashed lines indicate the selected electron range used in the Ar-Kr^+ ion source selection routine [59–61]. The color map is normalized to its peak value. (b) Measured electron momentum distribution of the doubly ionized Ar-Kr, where the white dashed sectors indicate the electron released by the elliptically polarized probe laser pulse. (c) The measured probe pulse liberated electron momentum distribution with the Ar-Kr^+ oriented as sketched in the inset. The first electron is selected from the pump pulse liberated with a ion momentum gating of $|\phi_{\rm ion}^{\rm rel}| < 30°$ and $pz_{\rm sum}^{\rm ion} > 0.3$ a.u., where $\phi_{\rm ion}^{\rm rel} = \arctan(pz_{\rm ion}^{\rm rel}/py_{\rm ion}^{\rm rel})$, and $p_{\rm ion}^{\rm rel} = p_{\rm ion}^{\rm Ar+} - p_{\rm ion}^{\rm Kr+}$. (d) The same as (c) but for theoretically calculated results. (e) The measured and simulated PADs in the polarization plane for $pz_e < 0$, where exp.1 and exp.2 correspond to the electron kinetic energy ranges in 6–12 and 5–16 eV, respectively. The blue solid lines are the fitting curves. The local maxima are labeled with dashed lines in (c) and (d). The green and orange areas show the direct and resonant ionization-pathway-resolved PADs.

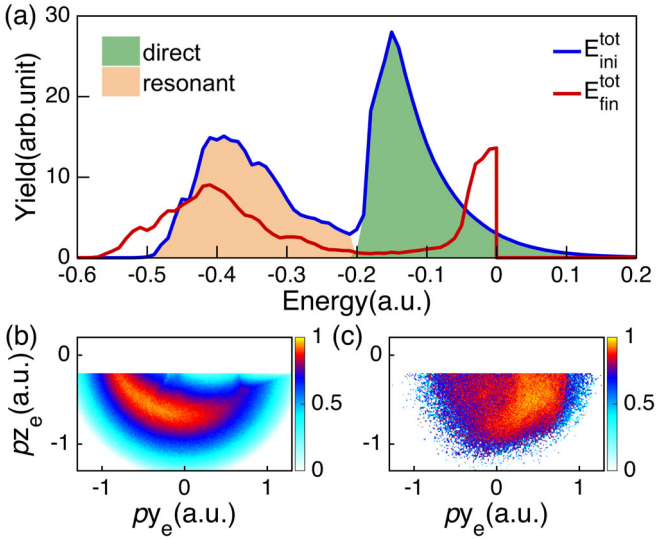

FIG. 3. (a) Theoretically calculated electron total energy distribution by summing over kinetic and potential energies. The blue curve shows the initial total energy distribution of the released electron $E_{\rm ini}^{\rm tot}$ at the tunneling exit, and the red curve shows the final total energy distribution of electrons with negative energy after the interaction with the laser field. (b) Direct and (c) resonant ionization-pathway-resolved electron momentum distributions, corresponding to the green and orange areas in (a), and the molecular orientation is the same as in Fig. 2(d).

typical resonant ionization process [see Fig. 1(d)]. The electron mainly tunnels through the internal barrier and emerges between the two ionic cores of the Ar^+ and Kr^+. The Coulomb interaction of the two ionic cores causes an additional trapping process to the electron before entering in the continuum with final energy $E_{\rm fin}^{\rm tot} > 0$. Figures 3(b) and 3(c) show the final electron momentum distributions corresponding to $E_{\rm ini}^{\rm tot} > -0.20$ a.u. and $E_{\rm ini}^{\rm tot} < -0.20$ a.u., i.e., the direct and resonant ionization processes, respectively. Figure 2(e) shows the integrated PADs with the color label the same as in Fig. 3(a). The local peak positions compare well to the measurement.

To figure out the intermediate trapping state, we analyze the final energy distribution of the electron with $E_{\rm fin}^{\rm tot} < 0$ after the interaction with the laser field [the red curve in Fig. 3(a)]. Its final energy distribution shows two peaks at $E_{\rm fin}^{\rm tot} = -0.40$ a.u. and -0.01 a.u. The typical electron trajectories with $E_{\rm fin}^{\rm tot} = -0.40$ a.u. are shown as the purple curve of Fig. 1(c). After tunneling through the internal barrier, the electron is tightly trapped by the ionic cores showing up many stabilized periodic trajectories (see more details in Supplemental Material [43]). The time-dependent total energy evolution of such trajectories shown in Fig. 4(a) confirms that the total energy almost keeps constant and remains negative around -0.40 a.u. Therefore, the peak of the final energy distribution of the electron with negative energy -0.40 a.u. is an excited state, and the arrow $T_{\rm ex}$ in Fig. 1(c) indicates the resonant excitation to the excited state. The overlapping between energy distributions of blue and red curves in Fig. 3(a) indicates that the photoelectron is first excited to the same trapping state as that of the electron with $E_{\rm fin}^{\rm tot} < 0$, and the blue-shifted energy distribution is induced by the Stark-shift effect of the laser field [67] (see also Supplemental Material [43]). As compared to the excitation process, the resonant ionization electron is trapped within the wells only for a period of time and gets freed eventually.

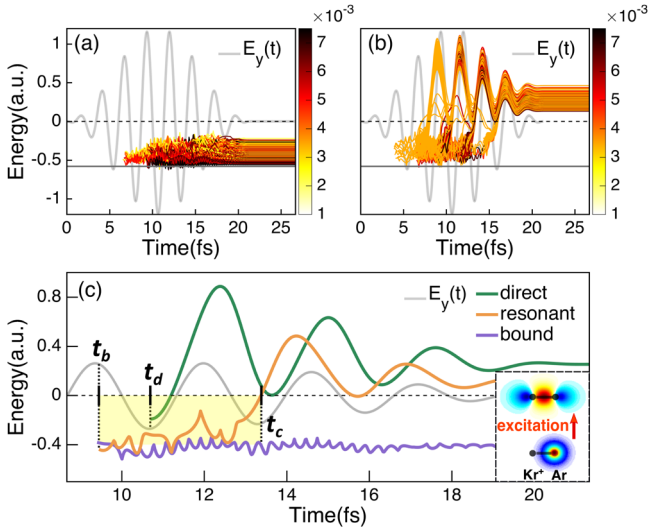

FIG. 4. (a) and (b) Time-dependent total energy evolution of the electron trajectories from (a) the excitation path and (b) the resonant tunneling ionization path. The electron trapping time corresponds to the platform with total energy around −0.40 a.u., and the colors show the probability of each trajectory. (c) The same as (a),(b) but for the typical electron trajectories presented in Figs. 1(a), 1(c), and 1(d). The gray lines in (a)–(c) show the electric field along the major axis of the elliptically polarized probe laser field. The inset in (c) shows the calculated electron wave functions of the ground state and resonant excited state of the Ar-Kr^+.

The difference between the resonant excitation and resonant ionization processes can be clearly seen from the time-dependent total energy evolution of electron trajectories as shown in Figs. 4(a) and 4(b). The semiclassical electron trajectory analysis clearly illustrates the nonadiabatic ionization proposed in [23]. It is that the tunneling of the trapped electron to the continuum through the internal barrier is thought to be the origin of the enhanced ionization, which is identical to the significant role of nonadiabatic resonant ionization in our theoretical simulations. Quantum mechanically, the enhanced ionization has contributed to the field-induced nonadiabatic transitions between the charged-resonant states [24], which is also related to the autoionization state in [68–70]. When the subbarrier Coulomb interaction is switched off in the simulations, the resonant excitation and resonant ionization would disappear (see the Supplemental Material [43]), which provides an alternative identification of the Coulomb trapping dynamics. In addition, the peak with $E_{\mathrm{fin}}^{\mathrm{tot}} \sim -0.01$ a.u. in Fig. 3(a) is related to the frustrated tunneling ionization, where the electron is first liberated into the continuum and then trapped into the high Rydberg states in the form of periodic elliptical trajectories (see the details in Supplemental Material [43]) [71,72].

To extract the time delay of the resonant trapping in the excited state, we employ the angular streaking deflection angle of the direct ionization pathway as a timing reference. Since both the nonadiabatic excitation and direct tunneling are almost instantaneous [73,74], and the angular shifts induced by the long-range Coulomb potential in the continuum are approximately equal for resonant and direct ionization, they effectively cancel each other. Therefore, the time delay of the resonant trapping process can be reconstructed by adopting the direct electron as a reference.

Nonadiabatic tunneling through the inner barrier mainly occurs when the instantaneous laser field points from Kr^+ to Ar. The "time zero" of the highest probability signal of the resonant ionization pathway is a half-cycle earlier than that of the direct ionization pathway (see Fig. S11 in the Supplemental Material [43]). The trapping process induces an additional offset of the deflection angle θ_f^r corresponding to the resonant time delay in the resonant state [the yellow area in Fig. 4(c), i.e., from the beginning of the trajectory to the time instant that the total energy reaches to zero]. The resonant time delay can be determined via $\Delta\theta = |\theta_f^r| - |\theta_f^d|$. The experimentally measured deflection angles of the direct and resonant ionization pathways are $\theta_f^d = 32° \pm 5°$ and $\theta_f^r = 144° \pm 5°$. Regarding the multicycle property of the driving laser pulse, the electron could be trapped in the resonant state for more than one optical period. Therefore, the offset angle induced by the resonant trapping should be generalized as $\Delta\theta_{\mathrm{exp}} = |\theta_f^r| - |\theta_f^d| + n \times 2\pi$, where n is an integer number. In the time domain, the deflection angle difference $\Delta\theta_{\mathrm{exp}} = (112° + n \times 360°) \pm 5°$ corresponds to a resonant time delay of $\tau_{\mathrm{exp}}^r = (0.83 + n \times 2.67) \pm 0.04$ fs.

We utilize the statistically averaged treatment on electron trajectories to clarify the unknown value of n in $\Delta\theta_{\mathrm{exp}}$ or τ_{exp}^r [13]. The resonant time delay can be calculated by the statistically averaged resonant time as $\langle\tau_{\mathrm{theo}}^r\rangle = \{[\sum_{j=1}^n \tau_{\mathrm{theo}}^r(j) \cdot W(j)]/\sum_{j=1}^n W(j)\}$, where $\tau_{\mathrm{theo}}^r = t_c(j) - t_b(j)$, with $t_b(j)$ and $t_c(j)$ as the time of electron emerging in the resonant state and the continuum, and $W(j)$ is the weight of the trajectory j, respectively. The averaged resonant time delay $\langle\tau_{\mathrm{theo}}^r\rangle = 3.57$ fs. Consistent with the molecular charge resonant enhanced ionization [23–25], the resonant time delay is sensitive to the internuclear separations and molecular orientation [15], and the maximum shift is about 0.2 fs within an orientation angle range of ±15°. The attoclock takes the angle of the highest probability signal as a clock hand, and the clock hand would rotate 360° over one optical period. Therefore, if the measured time delay is longer than one optical period, the measured offset should be plus $n \times 360°$. The simulated resonant time delay is longer than one optical period but shorter than two periods. And when $n = 1$, according to the experimentally measured offset, the reconstructed time delay is 3.50 fs, which is quite close to that obtained with 3.57 fs in the statistically averaged treatment of improved CCSFA.

In conclusion, by constructing a self-referenced molecular attoclock, we experimentally and theoretically demonstrated

a resonant time delay of 3.50 ± 0.04 fs in the ionization of Ar-Kr^+. The molecular attoclock unambiguously deflects the direct and resonant ionization pathways into two streaking angles in the PADs. The direct tunneling pathway provides a timing reference to calibrate the deflection angle from the laser-Coulomb coupling effect [6,9,10,16]. The statistical analyses based on electron trajectories provide a semiclassical landscape of the resonant ionization, which is interpreted in terms of the dynamics of the electron wave packet trapped in an intermediate state. The proposed self-referenced molecular attoclock approach opens up a new avenue for exploring the key role of neighboring Coulomb potential in the underbarrier electron tunneling dynamics and probing the lifetime of resonant states in the photoionization dynamics of complex molecules, and will hopefully spur more interesting works, such as the attosecond time-resolved auger decay and electron correlation based on the XFELs-IR pump-probe measurements [75].

This work was supported by the National Key R&D Program of China (Grant No. 2018YFA0306303), the National Natural Science Foundation of China (Grants No. 11761141004, No. 12122404, No. 11834004, No. 91950101, No. 12074240, No. 11974114), the Shanghai Science and Technology Commission (Grants No. 19JC1412200, No. 18ZR1412400, No. 19560745900), and the 111 Project of China (Grant No. B12024), the Fundamental Research Funds for the Central Universities, and the Sino-German Center for Research Promotion (SGC, Grant No. M-0031).

*These authors contributed equally to this work.
†xcgong@lps.ecnu.edu.cn
‡wfyang@hainanu.edu.cn
§jwu@phy.ecnu.edu.cn

[1] M. Dantus, M. J. Rosker, and A. H. Zewail, J. Chem. Phys. **87**, 2395 (1987).
[2] M. Uiberacker, T. Uphues, M. Schultze, A. J. Verhoef, V. Yakovlev, M. F. Kling, J. Rauschenberger, N. M. Kabachnik, H. Schröder, M. Lezius, K. L. Kompa, H. G. Muller, M. J. J. Vrakking, S. Hendel, U. Kleineberg, U. Heinzmann, M. Drescher, and F. Krausz, Nature (London) **446**, 627 (2007).
[3] D. Polli, P. Altoè, O. Weingart, K. M. Spillane, C. Manzoni, D. Brida, G. Tomasello, G. Orlandi, P. Kukura, R. A. Mathies, M. Garavelli, and G. Cerullo, Nature (London) **467**, 440 (2010).
[4] P. M. Kraus, B. Mignolet, D. Baykusheva, A. Rupenyan, L. Horný, E. F. Penka, G. Grassi, O. I. Tolstikhin, J. Schneider, F. Jensen, L. B. Madsen, A. D. Bandrauk, F. Remacle, and H. J. Wörner, Science **350**, 790 (2015).
[5] H. J. Wörner, J. B. Bertrand, D. V. Kartashov, P. B. Corkum, and D. M. Villeneuve, Nature (London) **466**, 604 (2010).
[6] R. Pazourek, S. Nagele, and J. Burgdörfer, Rev. Mod. Phys. **87**, 765 (2015).
[7] P. M. Paul, E. S. Toma, P. Breger, G. Mullot, F. Augé, P. Balcou, H. G. Muller, and P. Agostini, Science **292**, 1689 (2001).
[8] J. Itatani, F. Quéré, G. L. Yudin, M. Y. Ivanov, F. Krausz, and P. B. Corkum, Phys. Rev. Lett. **88**, 173903 (2002).
[9] M. Schultze *et al.*, Science **328**, 1658 (2010).
[10] P. Eckle, A. N. Pfeiffer, C. Cirelli, A. Staudte, R. Dörner, H. G. Muller, M. Büttiker, and U. Keller, Science **322**, 1525 (2008).
[11] A. S. Landsman, M. Weger, J. Maurer, R. Boge, A. Ludwig, S. Heuser, C. Cirelli, L. Gallmann, and U. Keller, Optics **1**, 343 (2014).
[12] X. Gong, C. Lin, F. He, Q. Song, K. Lin, Q. Ji, W. Zhang, J. Ma, P. Lu, Y. Liu, H. Zeng, W. Yang, and J. Wu, Phys. Rev. Lett. **118**, 143203 (2017).
[13] X. Song, G. Shi, G. Zhang, J. Xu, C. Lin, J. Chen, and W. Yang, Phys. Rev. Lett. **121**, 103201 (2018).
[14] U. S. Sainadh, H. Xu, X. Wang, A. Atia-Tul-Noor, W. C. Wallace, N. Douguet, A. Bray, I. Ivanov, K. Bartschat, A. Kheifets, R. T. Sang, and I. V. Litvinyuk, Nature (London) **568**, 75 (2019).
[15] J. Yan, W. Xie, M. Li, K. Liu, S. Luo, C. Cao, K. Guo, W. Cao, P. Lan, Q. Zhang, Y. Zhou, and P. Lu, Phys. Rev. A **102**, 013117 (2020).
[16] J. M. Dahlström, D. Guénot, K. Klünder, M. Gisselbrecht, J. Mauritsson, A. L'Huillier, A. Maquet, and R. Taïeb, Chem. Phys. **414**, 53 (2013).
[17] Z. Tao, C. Chen, T. Szilvási, M. Keller, M. Mavrikakis, H. Kapteyn, and M. Murnane, Science **353**, 62 (2016).
[18] M. Huppert, I. Jordan, D. Baykusheva, A. von Conta, and H. J. Wörner, Phys. Rev. Lett. **117**, 093001 (2016).
[19] X. Gong, W. Jiang, J. Tong, J. Qiang, P. Lu, H. Ni, R. Lucchese, K. Ueda, and J. Wu, Phys. Rev. X **12**, 011002 (2022).
[20] J. Su, H. Ni, A. Jaroń-Becker, and A. Becker, Phys. Rev. Lett. **113**, 263002 (2014).
[21] J. Vos, L. Cattaneo, S. Patchkovskii, T. Zimmermann, C. Cirelli, M. Lucchini, A. Kheifets, A. S. Landsman, and U. Keller, Science **360**, 1326 (2018).
[22] L. S. Cederbaum and J. Zobeley, Chem. Phys. Lett. **307**, 205 (1999).
[23] Tamar Seideman, M. Yu. Ivanov, and P. B. Corkum, Phys. Rev. Lett. **75**, 2819 (1995).
[24] T. Zuo and A. D. Bandrauk, Phys. Rev. A **52**, R2511 (1995).
[25] S. Chelkowski, T. Zuo, O. Atabek, and A. D. Bandrauk, Phys. Rev. A **52**, 2977 (1995).
[26] J. Wu, M. Meckel, L. P. H. Schmidt, M. Kunitski, S. Voss, H. Sann, H. Kim, T. Jahnke, A. Czasch, and R. Dörner, Nat. Commun. **3**, 1113 (2012).
[27] D. Trabert, S. Brennecke, K. Fehre, N. Anders, A. Geyer, S. Grundmann, M. S. Schöffler, L. P. H. Schmidt, T. Jahnke, R. Dörner, M. Kunitski, and S. Eckart, Nat. Commun. **12**, 1697 (2021).
[28] C. Y. Ng, P. W. Tiedemann, B. H. Mahan, and Y. T. Lee, J. Chem. Phys. **66**, 5737 (1977).
[29] P. M. Dehmer and S. T. Pratt, J. Chem. Phys. **77**, 4804 (1982).
[30] E. Kleimenov, L. Piticco, and F. Merkt, Mol. Phys. **106**, 1835 (2008).

[31] K. Gokhberg, P. Kolorenč, A. I. Kuleff, and L. S. Cederbaum, Nature (London) **505**, 661 (2014).
[32] C. F. Bender and N. W. Winter, Appl. Phys. Lett. **33**, 29 (1978).
[33] R. A. Aziz and A. Van Dalen, J. Chem. Phys. **78**, 2413 (1983).
[34] T. P. Haley and S. M. Cybulski, J. Chem. Phys. **119**, 5487 (2003).
[35] T. Miteva, Y.-C. Chiang, P. Kolorenč, A. I. Kuleff, L. S. Cederbaum, and K. Gokhberg, J. Chem. Phys. **141**, 164303 (2014).
[36] W. Fakhardji, P. Szabó, M. S. El-Kader, A. Haskopoulos, G. Maroulis, and M. Gustafsson, J. Chem. Phys. **151**, 144303 (2019).
[37] J. Wu, M. Magrakvelidze, A. Vredenborg, L. P. H. Schmidt, T. Jahnke, A. Czasch, R. Dörner, and U. Thumm, Phys. Rev. Lett. **110**, 033005 (2013).
[38] S. V. Popruzhenko, G. G. Paulus, and D. Bauer, Phys. Rev. A **77**, 053409 (2008).
[39] K. Mishima, M. Hayashi, J. Yi, S. H. Lin, H. L. Selzle, and E. W. Schlag, Phys. Rev. A **66**, 053408 (2002).
[40] W. Quan, X. L. Hao, Y. J. Chen, S. G. Yu, S. P. Xu, Y. L. Wang, R. P. Sun, X. Y. Lai, C. Y. Wu, Q. H. Gong, X. T. He, X. J. Liu, and J. Chen, Sci. Rep. **6**, 27108 (2016).
[41] R. Dörner, V. Mergel, O. Jagutzki, L. Spielberger, J. Ullrich, R. Moshammer, and H. Schmidt-Böcking, Phys. Rep. **330**, 95 (2000).
[42] J. Ullrich, R. Moshammer, A. Dorn, R. Dörner, L. P. H. Schmidt, and H. Schmidt-Böcking, Rep. Prog. Phys. **66**, 1463 (2003).
[43] See Supplemental Material at http://link.aps.org/supplemental/10.1103/PhysRevLett.129.173201 for kinetic energy release spectrum calibrated, details of the CCSFA method, Keldysh-Faisal-Reiss theory and the strong-field approximation, integration contour of the analytical R-matrix approach, and the Stark-shift effect, which includes Refs. [44–58].
[44] B. Ulrich, A. Vredenborg, A. Malakzadeh, M. Meckel, K. Cole, M. Smolarski, Z. Chang, T. Jahnke, and R. Dörner, Phys. Rev. A **82**, 013412 (2010).
[45] B. Manschwetus, H. Rottke, G. Steinmeyer, L. Foucar, A. Czasch, H. Schmidt-Böcking, and W. Sandner, Phys. Rev. A **82**, 013413 (2010).
[46] L. Poisson, K. D. Raffael, M. A. Gaveau, B. Soep, J. M. Mestdagh, J. Caillat, R. Taïeb, and A. Maquet, Phys. Rev. Lett. **99**, 103401 (2007).
[47] S. V. Popruzhenko and D. Bauer, J. Mod. Opt. **55**, 2573 (2008).
[48] Y. Huismans *et al.*, Science **331**, 61 (2011).
[49] L. V. Keldysh, Sov. Phys. JETP **20**, 1307 (1965), http://jetp.ras.ru/cgi-bin/e/index/e/20/5/p1307?a=list.
[50] F. H. Faisal, J. Phys. B **6**, L89 (1973).
[51] H. R. Reiss, Phys. Rev. A **22**, 1786 (1980).
[52] P. Salières, B. Carré, L. Le Déroff, F. Grasbon, G. G. Paulus, H. Walther, R. Kopold, W. Becker, D. B. Milošević, A. Sanpera, and M. Lewenstein, Science **292**, 902 (2001).
[53] A. M. Perelomov and V. S. Popov, Sov. Phys. JETP **25**, 336 (1967), http://jetp.ras.ru/cgi-bin/e/index/e/25/2/p336?a=list.
[54] L. Torlina and O. Smirnova, Phys. Rev. A **86**, 043408 (2012).
[55] T. Schultz and M. Vrakking, *Attosecond and XUV Physics: Ultrafast Dynamics and Spectroscopy* (Wiley-VCH, Weinheim, 2014).
[56] M. O. Scully and M. S. Zubairy, *Quantum Optics* (Cambridge University Press, Cambridge, 1997).
[57] N. Bleistein and R. A. Handelsman, *Asymptotic Expansions of Integrals* (Dover Publications, New York, 2010).
[58] A. Nayak *et al.*, Phys. Rep. **833**, 1 (2019).
[59] Q. Song, Z. Li, S. Cui, P. Lu, X. Gong, Q. Ji, K. Lin, W. Zhang, J. Ma, H. Pan, J. Ding, M. F. Kling, H. Zeng, F. He, and J. Wu, Phys. Rev. A **94**, 053419 (2016).
[60] S. Eckart, M. Kunitski, M. Richter, A. Hartung, J. Rist, F. Trinter, K. Fehre, N. Schlott, K. Henrichs, L. P. H. Schmidt, T. Jahnke, M. Schöffler, K. Liu, I. Barth, J. Kaushal, F. Morales, M. Ivanov, O. Smirnova, and R. Dörner, Nat. Phys. **14**, 701 (2018).
[61] X. Gong, P. He, J. Ma, W. Zhang, F. Sun, Q. Ji, K. Lin, H. Li, J. Qiang, P. Lu, H. Li, H. Zeng, J. Wu, and F. He, Phys. Rev. A **99**, 063407 (2019).
[62] Y. Mi, P. Peng, N. Camus, X. Sun, P. Fross, D. Martinez, Z. Dube, P. B. Corkum, D. M. Villeneuve, A. Staudte, R. Moshammer, and T. Pfeifer, Phys. Rev. Lett. **125**, 173201 (2020).
[63] R. P. Feynman, Rev. Mod. Phys. **20**, 367 (1948).
[64] X. Liu, G. Zhang, J. Li, G. Shi, M. Zhou, B. Huang, Y. Tang, X. Song, and W. Yang, Phys. Rev. Lett. **124**, 113202 (2020).
[65] T. M. Yan, S. V. Popruzhenko, M. J. J. Vrakking, and D. Bauer, Phys. Rev. Lett. **105**, 253002 (2010).
[66] T. Keil, S. V. Popruzhenko, and D. Bauer, Phys. Rev. Lett. **117**, 243003 (2016).
[67] N. B. Delone and V. P. Krainov, Phys. Usp. **42**, 669 (1999).
[68] X. Guan, K. Bartschat, B. I. Schneider, and L. Koesterke, Phys. Rev. A **88**, 043402 (2013).
[69] Y. Liu, L. Fu, D. Ye, J. Liu, M. Li, C. Wu, Q. Gong, R. Moshammer, and J. Ullrich, Phys. Rev. Lett. **112**, 013003 (2014).
[70] J. M. Ngoko Djiokap and A. F. Starace, Phys. Rev. A **103**, 053110 (2021).
[71] T. Nubbemeyer, K. Gorling, A. Saenz, U. Eichmann, and W. Sandner, Phys. Rev. Lett. **101**, 233001 (2008).
[72] B. Manschwetus, T. Nubbemeyer, K. Gorling, G. Steinmeyer, U. Eichmann, H. Rottke, and W. Sandner, Phys. Rev. Lett. **102**, 113002 (2009).
[73] L. Torlina, F. Morales, J. Kaushal, I. Ivanov, A. Kheifets, A. Zielinski, A. Scrinzi, H. G. Muller, S. Sukiasyan, M. Ivanov, and O. Smirnova, Nat. Phys. **11**, 503 (2015).
[74] H. Ni, U. Saalmann, and J. M. Rost, Phys. Rev. Lett. **117**, 023002 (2016).
[75] D. C. Haynes, M. Wurzer, A. Schletter, C. Blaga, and C. Bostedt, Nat. Phys. **17**, 512 (2021).